Materials Characterization 165 (2020) 110378

Contents lists available at ScienceDirect

Materials Characterization

journal homepage: www.elsevier.com/locate/matchar

Effect of heat treatment on microstructural evolution and creep behaviors of a conventionally cast nickel-based superalloy

In Soo Kim*, Baig-Gyu Choi, Joong Eun Jung, Jeonghyeon Do, Woo-Young Seok, You-Hwa Lee, In-Yong Jeong

High Temperature Materials Research Center, Korea Institute of Materials Science, 797 Changwon-daero, Changwon, Gyeongnam 51508, Republic of Korea

ARTICLE INFO

Keywords:
Superalloy
Heat treatment
γ′ precipitate
Eutectic phase
Creep behavior

ABSTRACT

The evolution of microstructures caused by heat treatment on Ni-based superalloy CM 247 LC was examined, and the creep behaviors were analyzed at various temperature and stress conditions. Secondary γ′ hardly precipitated in aged specimens subjected to solution treatment, but secondary γ′ precipitated in specimen subjected to two-step aging at 1080 °C and 871 °C without solution treatment, because the size and volume fraction of precipitated γ′ particles and the width of the γ channel depend on the heat-treatment path. The creep properties of the specimen subjected to two-step aging without solution heat treatment under low temperature and high stress was the best, owing to the uniform deformation and damage-relieving effect of the fine secondary γ′ particles in the γ channel and the eutectic γ/γ′ phase. At and above 871 °C, the effect of γ′ rafting on the creep properties was very important, and the creep lifetimes of the solution-treated specimens with better rafting were longer than those of the aged specimens.

1. Introduction

Many researches have been conducted on nickel-based superalloys for applications in high temperature equipment, such as gas turbines. For example, the CM 247 LC alloy has been applied to the blades in jet engines and in power generating gas turbines. The CM 247 LC alloy is a nickel-based superalloy developed by Cannon-Muskegon to supplement the composition of the superalloy Mar-M 247 developed for polycrystalline application and is used as a directional solidification alloy [1]. Superalloys have been developed into polycrystalline materials via directional solidification, and single crystal alloys with the development of vacuum precision casting process technology, with many studies having been made to improve the mechanical properties of these alloys through optimization in the sizes, shapes and distributions of γ′ particles [2,3]. The CM 247 LC alloy was developed as a directional solidification alloy, and has been applied to polycrystalline castings such as for integral turbine rotors by suppressing casting defects such as hot cracking [4,5]. The creep deformation mechanisms of superalloys vary with the particle shearing by super-dislocation or stacking fault and the dislocation climb, depending on the temperature and stress [6,7]. Many studies have been conducted to improve the tensile and creep properties of superalloys and to optimize the application of components by controlling the heat-treatment process [8,9]. The solution temperature (solvus) of the γ′ particles of the CM 247 LC alloy is 1249 °C, whereas the incipient melting point is about 1257 °C in a single step solution process, and about 1270 °C when pre-homogenization is performed [4]. Efficient solution treatment of the DS CM 247 LC alloy can be performed by step-solution, i.e., effective homogenization of cast and segregated microstructures prior to the final solution at high temperatures. An effective homogenization treatment increases the incipient melting point of the alloy, thus widening the range of the possible final heat-treatment temperature, which maximizes the solution of the eutectic γ/γ′ microstructure. Excellent mechanical properties can be obtained by maximizing precipitation of the fine γ′ particles that contribute to the strength of the alloy [4]. The fine γ′ particles obtained by precipitation after the solution treatment inhibit the dislocation movement more effectively than the coarse as-cast γ′ phase does and have a volume fraction of about 65% in the CM 247 LC alloy [10].

As previously stated, studies on heat treatment to improve the properties of CM 247 LC alloy have been conducted. However, very few studies have clearly described the effect of heat treatment on microstructure such as γ′ precipitation behavior and dissolution of eutectic γ/γ′ phase, and how these evolutions of microstructure affect creep properties. Therefore, in this study, we examined the evolution of the microstructure, especially the precipitation of γ′ and dissolution of

* Corresponding author.
E-mail address: kis@kims.re.kr (I.S. Kim).

https://doi.org/10.1016/j.matchar.2020.110378
Received 21 February 2020; Received in revised form 23 April 2020; Accepted 9 May 2020
Available online 11 May 2020
1044-5803/ © 2020 Elsevier Inc. All rights reserved.

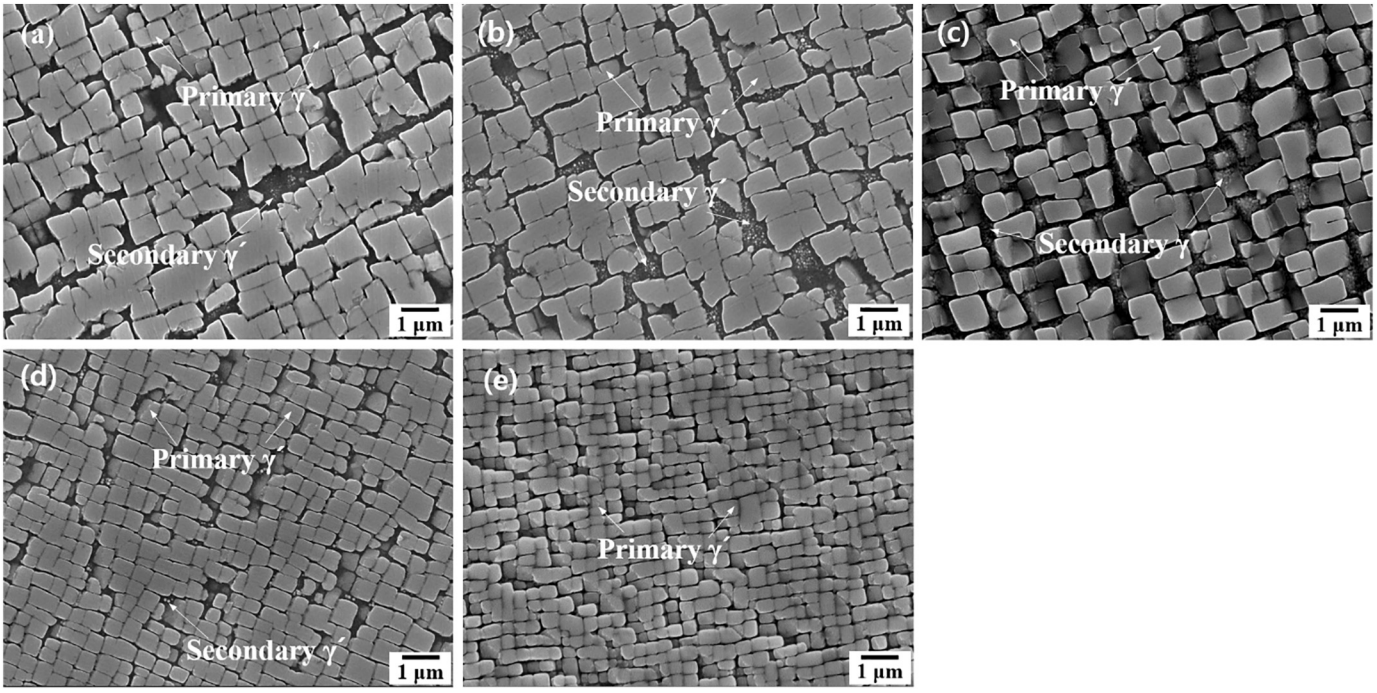

Fig. 1. Morphologies of γ′ particles in as-cast and heat treated CM247LC: (a) as-cast, (b) HT1, (c) HT2, (d) HT3, and (e) HT4 specimens.

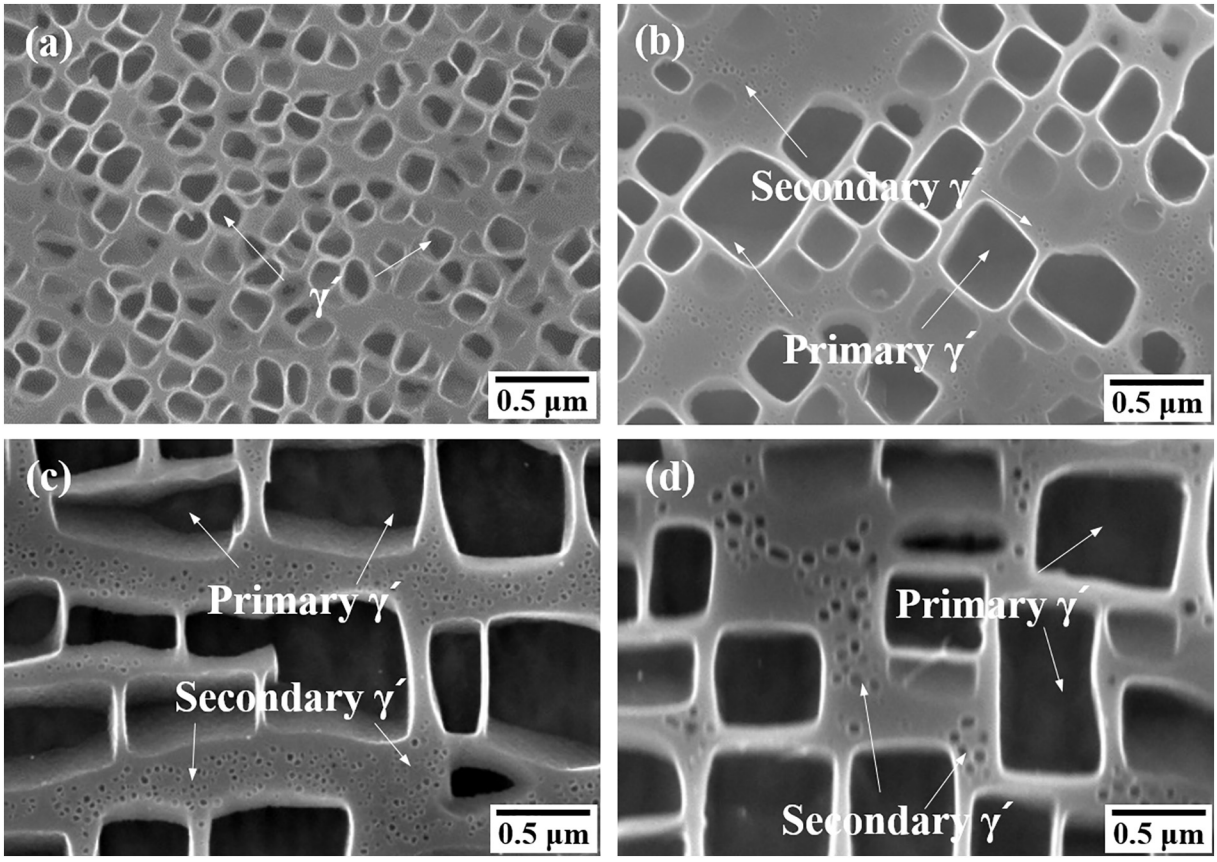

Fig. 2. Morphologies of γ′ particles in heat treated CM247LC: (a) 1232 ˚C/2 h/AC, (b) 1232 ˚C/2 h/AC + 1080 ˚C/4 h/AC, (c) 1080 ˚C/4 h/AC, (d) 1080 ˚C/4 h/AC + 871 ˚C/20 h/AC (HT3).

eutectic γ/γ′ phase, with respect to the heat treatment of CM 247 LC alloy, and investigated how the process affects creep deformation at various testing conditions. Other phases that contribute to the deformation of the alloy are carbides. Precipitated $M_{23}C_6$ carbide at the grain boundary, for example, inhibits grain boundary sliding when the alloy deforms at high temperatures [11]. In this study, however, the alloy composition was the same, and the precipitation behavior of carbides after aging treatment was not very different. Therefore, the

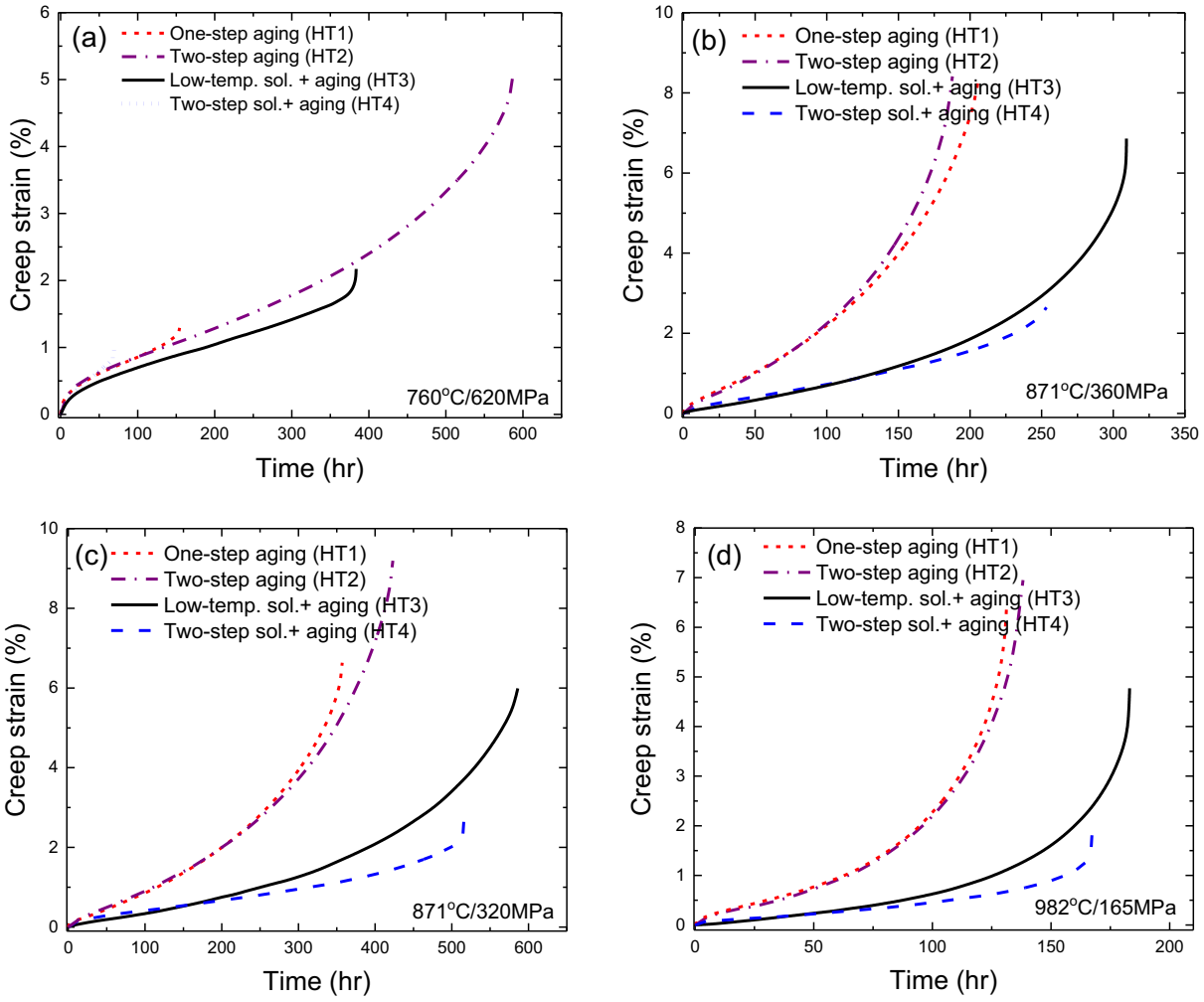

Fig. 3. Creep curves with respect to heat treatments at various testing conditions: (a) 760 °C/620 MPa, (b) 871 °C/360 MPa, (c) 871 °C/320 MPa, (d) 982 °C/165 MPa.

difference in creep behavior caused by carbides is insignificant. The main issue of this study was limited to the relation between creep behavior and the evolution of the γ′ particle, which is the principal strengthening phase.

2. Experimental procedure

Cylindrical specimens 80 mm in length and 12.5 mm in diameter were cast in a vacuum induction furnace using a commercial CM247LC alloy ingot (Ni-0.07C-0.015B-0.015Zr-5.6Al-1.4Ti-8.1Cr-9.2Co-0.5Mo-9.5W-3.2Ta-1.4Hf in wt%) purchased from Cannon-Muskegon. The cast specimens were subjected to various types of heat treatments to investigate the microstructural evolution and creep behavior with respected to the heat treatment. The heat treatment used in this experiment is based on the heat treatment generally used for Mar-M 247 and CM247LC alloys [10].

1) HT1: 871 °C/20 h/AC (one-step aging)
2) HT2: 1080 °C/4 h/AC + 871 °C/20 h/AC (two-step aging)
3) HT3: 1232 °C/2 h/AC + 1080 °C/4 h/AC + 871 °C/20 h/AC (low-temperature solution)
4) HT4: 1232 °C/2 h + 1260 °C/2 h/AC + 1080 °C/4 h/AC + 871 °C/20 h/AC (two-step solution)

Using a constant load creep tester manufactured by ATS, creep tests were performed on the heat-treated specimens at temperatures between 760 °C and 982 °C, where the cylindrical specimens each had a gauge length of 25 mm and a gauge diameter of 6 mm.

Creep-fractured specimens or interrupted specimen, obtained from creep test that was ceased prior to failure due to creep deformation, were cut parallel to the direction of stress, and the surfaces were polished to examine the microstructures, which were then compared with the microstructures that were viewed immediately after heat treatment. Electrolytic etching for microstructural observation was performed in 100 ml of CrO_3 3 g + H_2O solution or 33% acetic acid, when the γ′ particles were observed to exhibit dissolution of the γ matrix. To dissolve the γ′ particle, it was etched using a 33% nitric acid + 33% distilled water + 1% hydrofluoric acid solution and observed with an optical microscope and a scanning electron microscope (Scanning Election Microscopy, SEM: JEOL JSM-7100F). To analyze the deformation state of the specimens via TEM (JEOL, JEM-2100F), thin foils were taken parallel to the direction of the loading axis. The foils were then polished in an electrolyte containing 10% perchloric acid and 7% glycerin in ethanol at 40 mA and −20 °C in a twin jet electro-polisher.

3. Results and discussions

3.1. Microstructure of CM247LC alloy after heat treatment

The morphologies of γ′ particles in the dendritic core region of the CM 247 LC alloy in the as-cast condition and after HT1–HT4 heat treatments are shown in Fig. 1. In the as-cast specimen, octocube-type

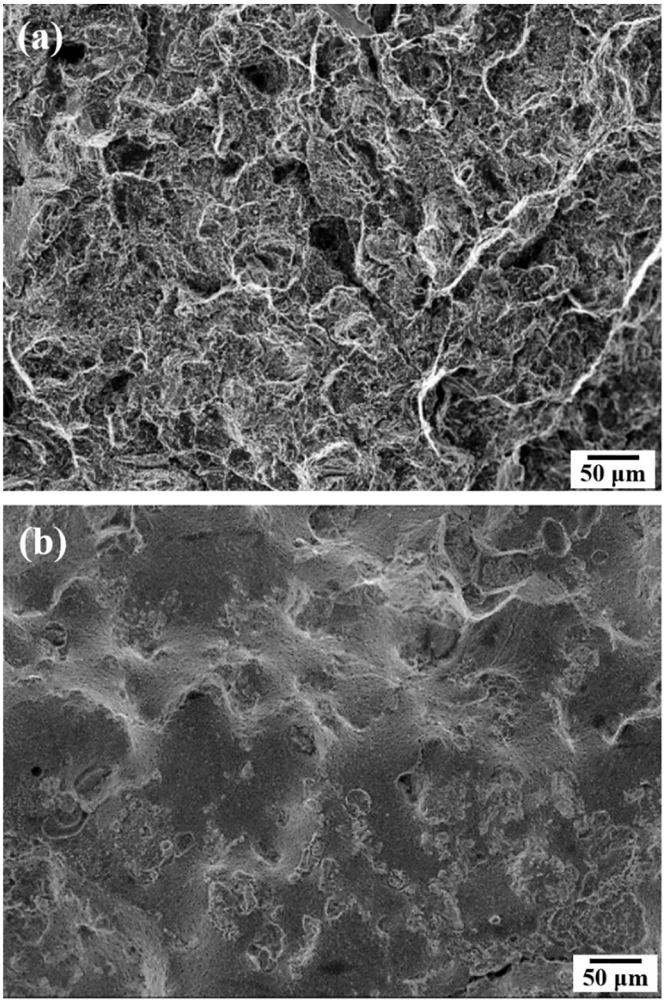

Fig. 4. Fractured surfaces of crept specimens: (a) 760 ˚C620 MPa, HT2 condition, (b) 871 ˚C/320 MPa, HT4 condition.

primary γ′ particles were formed, which were not separated into perfect cubes, and small amounts of very fine secondary γ′ particles precipitated in the γ channel. In the specimen heat-treated at 871 ˚C for 20 h (HT1, one-step aging), the morphology of primary γ′ did not change remarkably compared to that of the as-cast specimen, and although the amount and sizes of secondary γ′ particles increased slightly, there were no significant differences. In the specimen heat-treated at 1080 ˚C for 4 h and then aged at 871 ˚C for 20 h (HT2, two-step aging), the primary γ′ was changed from octocube to cube in the dendrite core, and a large amount of secondary γ′ (0.05–0.08 μm) precipitated in the γ channel. In the HT3 specimen, which had been subjected to solution treatment at a low temperature of 1232 ˚C and then aged at 1080 ˚C and 871 ˚C, 0.5–0.7 μm sized cube-type primary γ′ precipitated, and a few secondary γ′ precipitated in a relatively wide γ channel. About 0.4–0.6 μm sized cube-type primary γ′ precipitated in the HT4 specimen that, pre-solution, was heat-treated at 1232 ˚C, subjected to a final solution treatment at 1260 ˚C, and then aged at 1080 ˚C and 871 ˚C, but few secondary γ′ particles were observed. In general, to obtain the best creep properties, the optimum heat treatment process is to suppress incipient melting due to segregation via pre-solution heat treatment and to dissolve a larger amount of coarse eutectic γ/γ′ at a higher temperature to precipitate the maximum amount of fine γ′ [4].

As shown in Fig. 1, the experiment confirmed not only the shapes and sizes of the primary γ′ in the dendritic core region, but also the precipitation behavior of the secondary γ′ depending on the heat-treatment path. Even with the same aging treatment at 1080 ˚C and 871 ˚C, the precipitation behavior of secondary γ′ was completely different according to the solution treatment (Fig. 1(c)–(e)). As shown in Fig. 2(a), when the sample was cooled after solution heat treatment at 1232 ˚C, fine γ′ particles of about 0.2 μm size precipitated from a completely solutionized matrix in the dendritic core region. They grew into cube-shaped primary γ′, and very fine secondary γ′ particles of 0.01–0.03 μm size precipitated in the γ channel after this specimen was aged at 1080 ˚C, as shown in Fig. 2(b). When the specimen was aged at 871 ˚C, the primary γ′ particles became closer to a more perfect cube, and the fine secondary γ′ particles grew to form some relatively coarse secondary γ′ or were absorbed by the primary γ′ where the width of the γ channel was narrow, as shown in Fig. 1(d). On the other hand, if heat treatment was performed at 1080 ˚C without solution treatment, some octocube-type primary γ′ particles formed at a relatively slow cooling rate after casting were separated into cubes, such that some γ′ to be dissolved into a γ matrix to satisfy the equilibrium γ′ volume fraction at 1080 ˚C. When the specimen was cooled after heat treatment at 1080 ˚C, fine secondary γ′ of 0.02–0.04 μm size precipitated in γ matrix supersaturated with γ′-forming elements such as Al, Ti, and Ta, as shown in Fig. 2(c). The fine secondary γ′ particles grew to 0.05–0.09 μm when the specimen aged at 871 ˚C as shown in Fig. 2(d).

The equilibrium volume fraction of γ′ increases as temperature decreases, such that the volume fraction of γ′ phase increases during aging at 871 ˚C. In the case of aged specimens not subjected to solution-heat treatment, there are relatively more interdendritic regions or eutectic phases where more γ′-forming elements are segregated, such that the equilibrium γ′ volume fraction is smaller in the dendrite core region because there are fewer γ′-forming elements. Further, the size of γ′ is larger, as shown in Fig. 1(c), which resulted in wider γ channel. Therefore, secondary γ′ particles grow and remain in the channel rather than being absorbed into primary γ′ during secondary aging at 871 ˚C. By contrast, the higher volume fraction of primary γ′ more finely precipitates in the solution-treated specimen, and the width of the γ channel becomes narrower. The very fine γ′ precipitated during the 1080 ˚C heat-treatment cycle is more likely to be absorbed into existing primary γ′ particles than to grow as secondary γ′ particles during the 871 ˚C aging. The thickness of the γ channel noticeably affects the precipitation behavior of the secondary γ′ even when the secondary γ′ particles generally form at a wide γ channel, as shown in Fig. 2.

3.2. Creep behavior with heat treatment

Creep deformation curves of CM 247 LC alloy with various microstructures from different heat treatments were measured and drawn at low, intermediate and high temperatures, as shown in Fig. 3.

3.2.1. Creep behavior at low temperature (760 ˚C)

A distinct primary creep region appeared in all specimens regardless of heat treatment at 760 ˚C/620 MPa testing condition. HT2 specimen aged at 1080 ˚C and 871 ˚C and not subjected to solution treatment exhibited the longest creep life, followed by HT3 specimen subjected to aging after solution treatment at 1232 ˚C. The next was HT1 specimen subjected only to one-step aging at 871 ˚C, fellow by two-step-solution-treated HT4 specimen, which exhibited shortest creep life. Creep strains were also highest for the HT2 specimen and lowest for the HT4 specimen, following the same order for the length of creep life. In this creep testing condition, the creep strain was proportional to creep life. Specimens with more strain exhibited longer creep lives. The HT2 specimen exhibited a long tertiary stage after a relatively short steady-state creep region, whereas the HT3 specimen exhibited the lowest steady-state creep strain rates with a long steady-state creep region, and a short tertiary stage. The HT4 specimen had a minimum creep rate that was higher than that of the other heat-treated specimens, and appeared to fail through the tertiary stage immediately after the primary creep region, without the steady-state creep region.

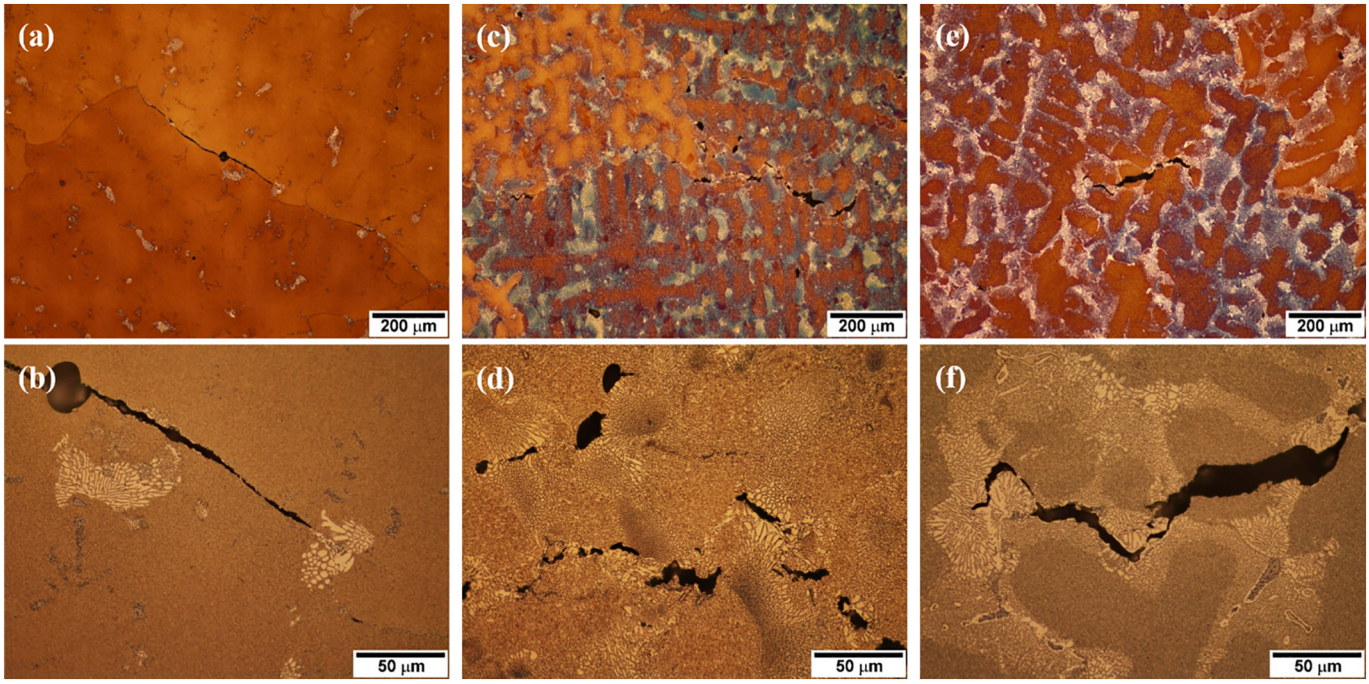

Fig. 5. Metallographic sectioning of crept specimen: (a) and (b) 871 °C/360 MPa, HT4 condition, (c) and (d) 871 °C/360 MPa, HT1 condition, (e) and (f) 982 °C/165 MPa, HT2 condition.

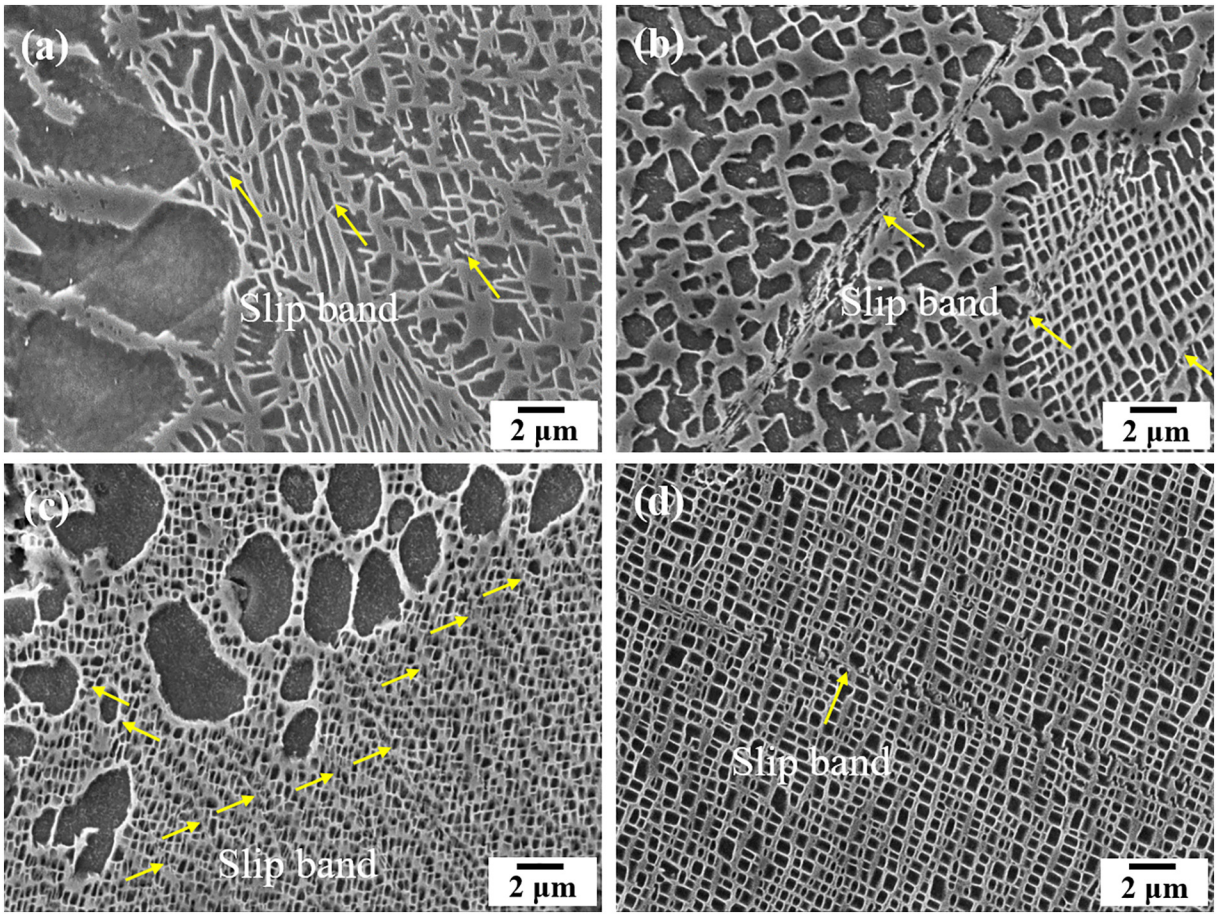

Fig. 6. Slip bands in crept specimens under 760 °C/620 MPa testing condition: (a) HT1, (b) HT2, (c) HT3, (d) HT4.

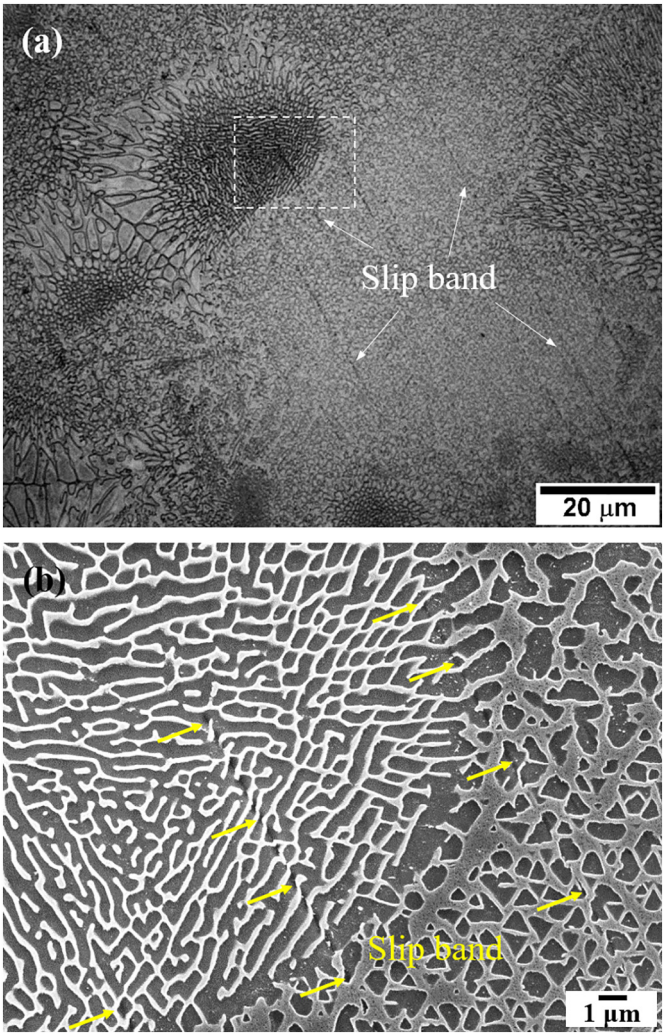

Fig. 7. Slip bands in interrupted specimen: (a) optical micrograph shows slip bands, (b) SEM micrograph shows slip bands stand in eutectic γ/γ′.

3.2.2. Creep behavior at intermediate temperature (871 °C)

At 871 °C, similar trends were exhibited for both stress conditions of 360 MPa and 320 MPa, and regardless of heat treatment, there was a short primary creep area and long tertiary creep region. The creep lives of the HT3 specimen were the longest, whereas the creep lives of the HT1 and HT2 specimens were short. Creep strains were high in the aged specimens that were subjected to solution-heat treatment, whereas HT4 specimens subjected to two-step solution-heat treatment exhibited the lowest creep strains. Unlike in the previous experiment, creep strain and life were not proportional. Generally, the solution-treated specimens had longer creep lives and less strain than the aged specimens not subjected to solution treatment. Steady-state creep was short, and tertiary creep regime was relatively long for all heat treatment conditions except for the HT4 specimens, which exhibited relatively long steady-state creep and short tertiary regions. At the same temperature, steady-state creep was long, and tertiary creep region was shorter at lower stress conditions.

3.2.3. Creep behavior at high temperature (982 °C)

Creep behaviors at the high temperature 982 °C were similar to those in 871 °C. Primary creep regime under the condition 982 °C/165 MPa was smaller than that at 871 °C. Primary creep strain was larger in the aged specimens not subjected to solution treatment than in the solution-treated specimens. Aged specimens not subjected to solution treatment exhibited acceleration of creep deformation through entrance into the tertiary creep region immediately after the primary creep, with a very short steady-state creep region. The HT3 specimen had the longest creep life, followed by the HT4 specimens, and whereas age-only specimens had the shortest lives.

3.3. Microstructural evolution during creep deformation

Regardless of temperature and stress, two types of fracture surfaces were observed upon heat treatment, as shown in Fig. 4. Specimens that did not demonstrate complete dissolution of eutectic γ/γ′ phase, such as HT1, HT2, and HT3, exhibited interdendritic fractures mode, as shown in Fig. 4(a), but the HT4 specimens, in which the eutectic γ/γ′ was almost completely dissolved, exhibited very smooth fractured surfaces and few ligaments or traces of deformation, as shown in Fig. 4(b). To reveal the reason behind such fractured surfaces, the crept specimens were metallographically sectioned in parallel to the stress axis to show the cracks that formed during creep, as shown in Fig. 5. In HT4 specimens with few eutectic γ/γ′ (volume fraction of eutectic phase was measured to be 1.6%), sharp cracks propagated along the grain boundaries as shown in Fig. 5(a). In other heat treated specimens with many eutectic γ/γ′ remaining (volume fractions of eutectic phase in as-cast and HT3 specimens were measured to be 15.9% and 13.0%, respectively), cracks propagated along dendritic boundaries within grains and along grain boundaries, as shown in Fig. 5(b) and (c). The cracks sometimes cut and passed through the eutectic γ/γ′, propagated along the boundary between the coarse eutectic γ′ and fine γ′ in the dendrite core region, and were rough and irregular in shape. Differences in microstructure caused intergranular fracture in the HT4 specimens and interdendritic fracture in the other heat treated specimens.

Fig. 6 shows the microstructure of creep fractured specimens at 760 °C/620 MPa after different heat-treatment processes. Under low temperature and high stress creep conditions, movements of dislocations were concentrated in local slip bands during creep deformation, regardless of heat treatment. The number of slip bands was very small in the HT4 specimen, whereas many slip bands formed in the other specimens, as shown in Fig. 6. Therefore, the creep curves in Fig. 3 shows that, in the HT4 specimen, unlike in the specimens subjected to other heat treatment conditions, the strain is found to be concentrated in a few slip bands, resulting in failure even at very low creep strain. The low number of slip bands in HT4 specimen can be attributed to many possible reasons, among which the absence of eutectic γ/γ′ may be the actual reason. Because the microstructures shown in Fig. 6 were observed in creep-ruptured specimens, most of the slip bands cut through eutectic γ/γ′ and the dendrite core regions because of excessive deformation, although some slip bands did not shear eutectic γ/γ′, as shown in Fig. 6(c). Therefore, to observe whether the eutectic γ/γ′ phase inhibits deformation, the interruption test was performed at 760 °C/620 MPa conditions using HT2 heat treated specimen. After the specimen was deformed to 2.97% at 481 h, the tertiary region, the test was stopped, and the microstructure was observed in a plane parallel to the stress direction. Fig. 7(a) shows an optical microstructure in which slip bands formed between the dendritic core region and eutectic γ/γ′ phases, whereas Fig. 7(b) shows the microstructure observed in an area corresponding to the rectangle in Fig. 7(a), enlarged with a scanning electron microscope. Some slip bands were confirmed to have stopped and to have not moved forward on eutectic γ/γ′. Because the eutectic phase suppresses slip-band progression, the reason why the creep life is longer for a specimen in which eutectic γ/γ′ is not completely dissolved could be elucidated.

The TEM microstructures (STEM mode) of creep-ruptured specimens with subjected to different heat treatments are shown in Fig. 8. The deformation was not homogeneous in the HT1 specimen, as shown in Fig. 8(a) and (b). When stress was applied, the dislocations moved first in the γ channel, and relatively more deformations formed in the wider channel, which resulted in stress concentration at the γ-γ′ interface, easily leading to the shearing of the γ′ particles. On the other

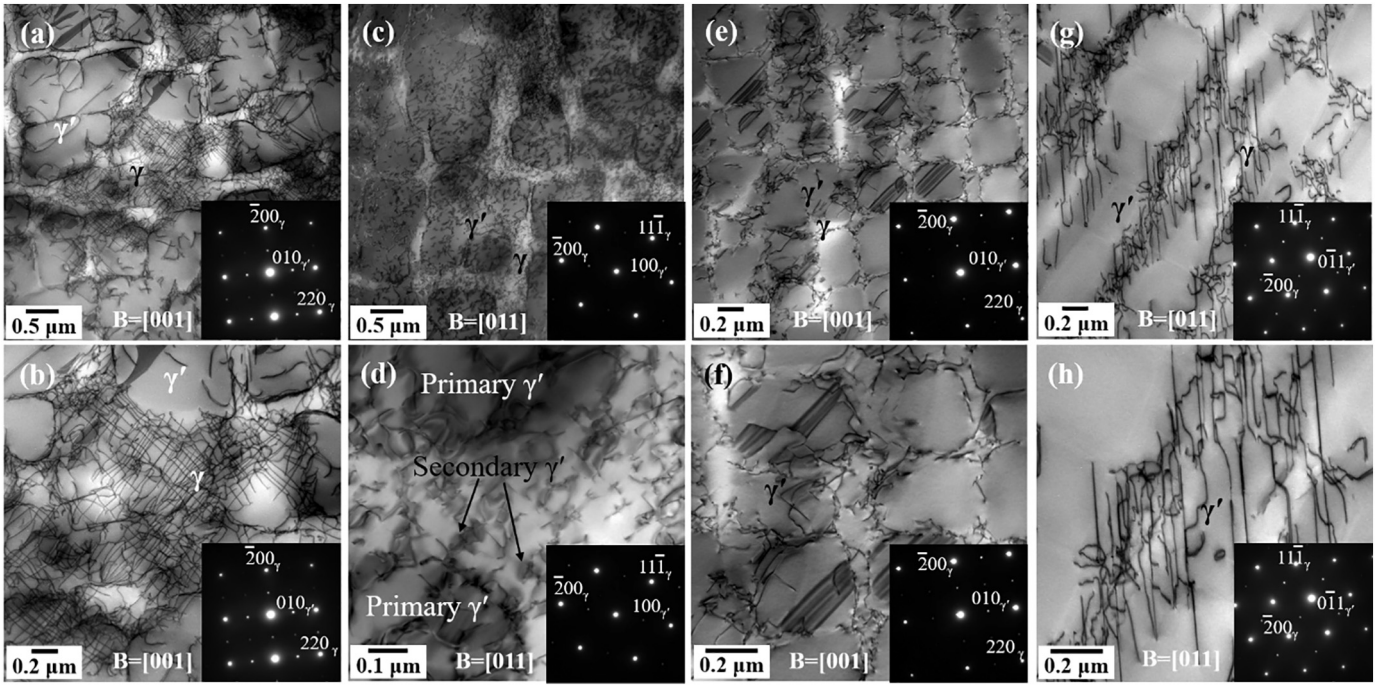

Fig. 8. TEM micrographs of crept specimens under 760 °C/620 MPa testing condition: (a), (b) HT1, (c), (d) HT2, (e), (f) HT3, (g), (h) HT4.

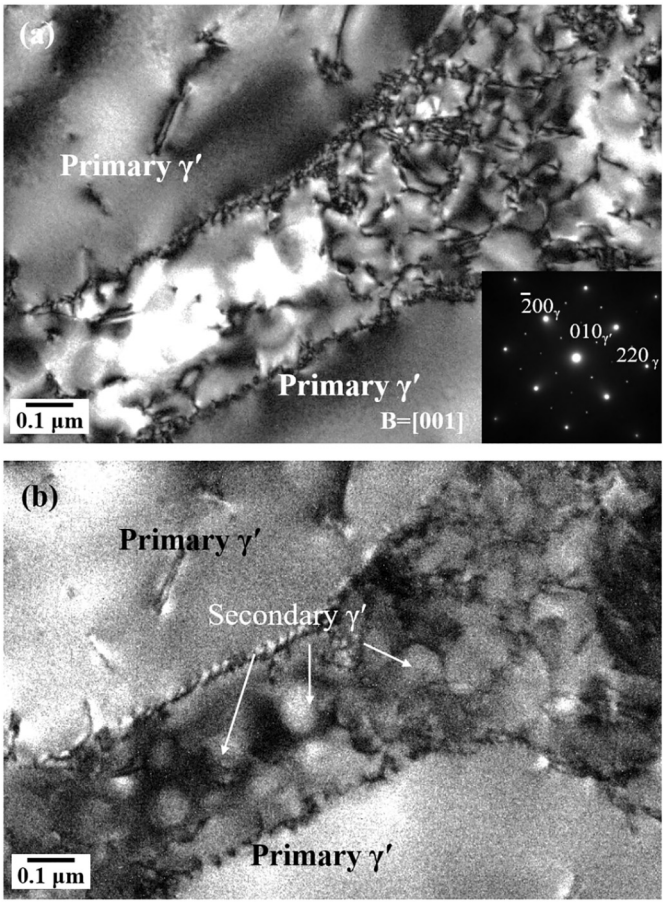

Fig. 9. TEM micrographs of crept HT2 specimens under 760 °C/620 MPa testing condition: (a) bright-field image, (b) dark-field image.

hand, as shown in Fig. 8(c) and (d), γ′ particles in the HT2 specimens were sheared by very short dislocation segments. Even within the γ channel, the dislocations were noticeably distributed homogeneously, such that the strain was uniform. Meanwhile, each γ′ in the HT3 specimen solution treated at low temperature was sheared by an isolated stacking fault, as shown in Fig. 8(e) and (f). Shearing of γ′ by isolated stacking fault occurs when the stacking fault energy is high, or when the width of γ channel is wide [12]. Insufficient solution caused to a relatively wider γ channel, resulting in the isolated stacking fault. For fully solution-treated HT4 specimen, the concentration of strain was noticeably larger and more uneven where several γ′ particles were continuously and sharply sheared by longer dislocations, than those carried by stacking faults within individual γ′ (Fig. 8(g) and (h)).

The interaction between secondary γ′ precipitated in the γ channel and dislocations of the creep-ruptured HT2 specimen at 760 °C/620 MPa were clearly observed in the TEM bright-field and dark-field images, as shown in Fig. 9. In the HT2 specimen, spherical secondary γ′ particles of about 0.1 μm size, which were precipitated in the γ channel during heat treatment, inhibited dislocation movement and prevented strain concentration. Fig. 10 shows the dislocation structure at the eutectic γ/γ′ of a creep-ruptured HT2 specimen at 760 °C/620 MPa. Fig. 10(a) and (b) was observed at the [011] zone, which is the same zone of observation as Fig. 8(c) and (d). Because the dislocation density or shape may depend on the zone axis, dislocation structures were also observed in the [001] zone of the specimen, as shown in Fig. 10(c) and (d). Primary γ′ was sheared by the high density of short dislocation segments in the dendrite core region, whereas eutectic γ′ was partially sheared by the quite low density of dislocation, and there were no significant differences in the different zone axes. In general, the eutectic γ/γ′ is a phase that improves ductility rather than strength [13] and is known to increase creep life by promoting crack blunting at grain boundaries [14] or by improving crack resistance at grain boundaries [15]. In this study, the eutectic γ/γ′ was found to act as a barrier to prevent dislocation movement when dislocation cut through the γ′ particles. The eutectic γ/γ′ suppressed the movement of the slip band and activated other slip bands, thereby playing an important role in extending the creep life by relieving stress concentration. The shortest creep life at 760 °C/620 Mpa, which was observed for HT4 specimen,

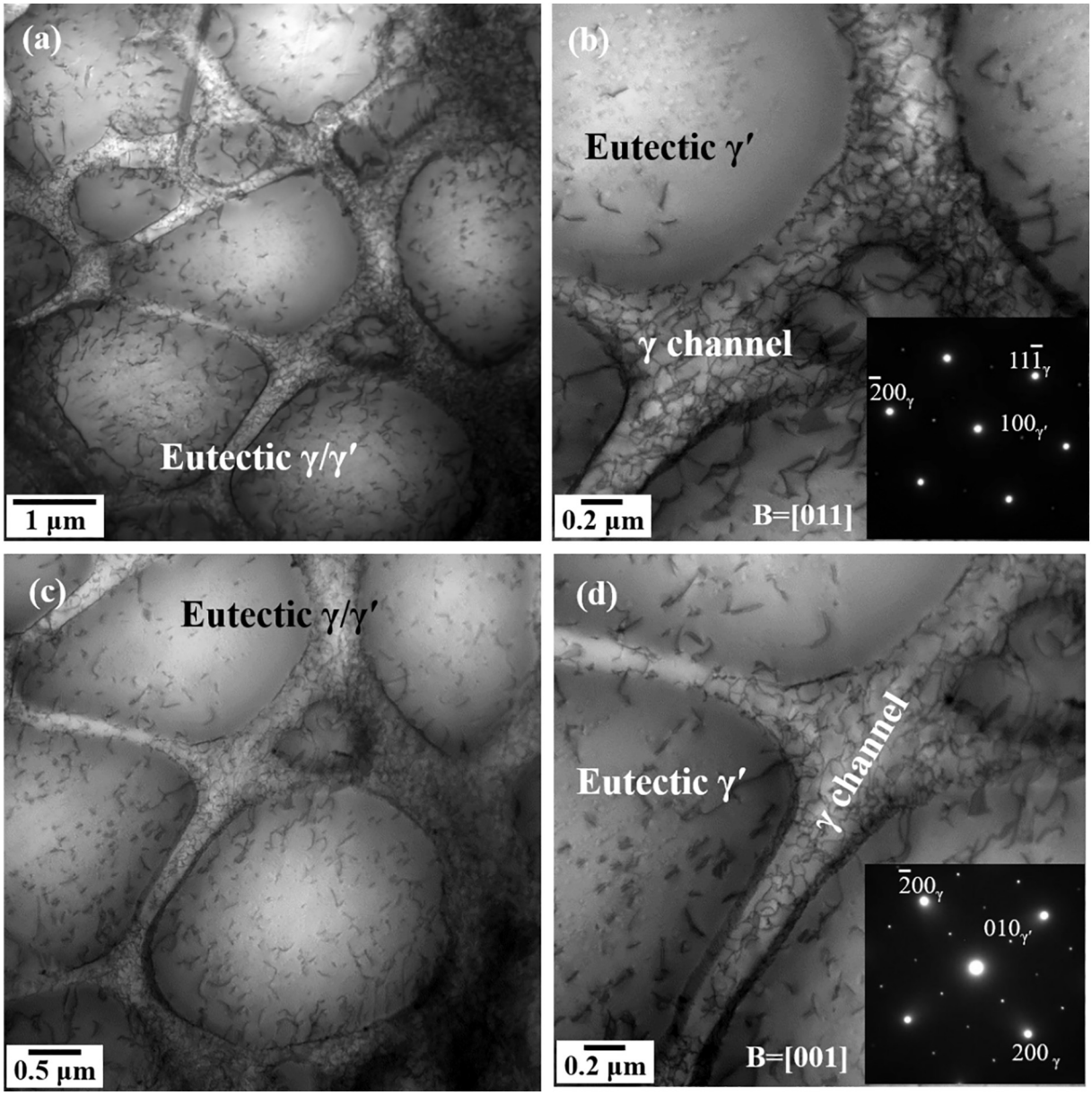

Fig. 10. TEM micrographs of crept HT2 specimens under 760 °C/620 MPa testing condition: (a), (b) [011] zone, and (c), (d) [001] zone.

was caused by the lack of eutectic γ/γ′. On the other hand, the longer creep life and larger elongation of the HT2 specimen at 760 °C/620 MPa are due to the eutectic γ/γ′ restraining the stress concentrations, and the secondary γ′ precipitating in the γ channel, which prevented the displacement of dislocations and relieved the stress concentration in the γ-γ′ interface as shown in Figs. 8 and 9.

The shapes of γ′ after creep tests at 871 °C/320 MPa and 982 °C/165 MPa are shown in Fig. 11. The creep deformation behaviors of this alloy at intermediate and high temperatures depended on the solution-heat treatment, as shown in Fig. 3. The microstructure after creep deformation was also clearly distinguished by the heat treatment. As shown in Fig. 11(a)–(c), γ′ particles maintained octocube or cube forms even though the aspect ratios of some of the γ′ particles increased slightly in the HT2 specimen, whereas rafting of γ′ particles was clearly observed in the HT3 and HT4 specimens. The rafting of the γ′ particles resulted in creep deformation being suppressed and the creep life being improved because it was difficult for the dislocations to pass through the γ′ [16]. Superalloys are generally deformed by shearing γ′ due to stacking faults or antiphase boundaries (APBs) shearing at low temperature and high stress. At high temperature and low stress, deformation occurs mainly because of the combined process of dislocation glide or climb in the γ channel, and some shearing of γ′ due to dislocation occurs [17,18]. The stable raft structure at high-temperature and low-stress condition suppresses the climb of dislocations and causes longer stress rupture life [19]. However, when stress is high, γ′ shear occurs because of coupled dislocation [20,21]. In this study, although rafting occurred even in aged specimens not subjected to solution treatment during high-temperature creeps at 982 °C, it was coarse and inhomogeneous compared to that in the solution-heat-treated specimens, as shown in Fig. 11(d). No secondary γ′ was found in the γ channel in any of the specimens, because growth at high temperatures caused aggregation of several relatively coarse secondary γ′ or coalescing into neighboring primary γ′. In addition to the absence of secondary γ′, the degree of rafting was a very important factor in creep deformation at temperatures above 871 °C. Through the suppression of the bypass mechanism of dislocations, strain rates were decreased and creep lives were extended. Because the HT1 and HT2 specimens exhibited almost similar creep behaviors at temperatures above 871 °C,

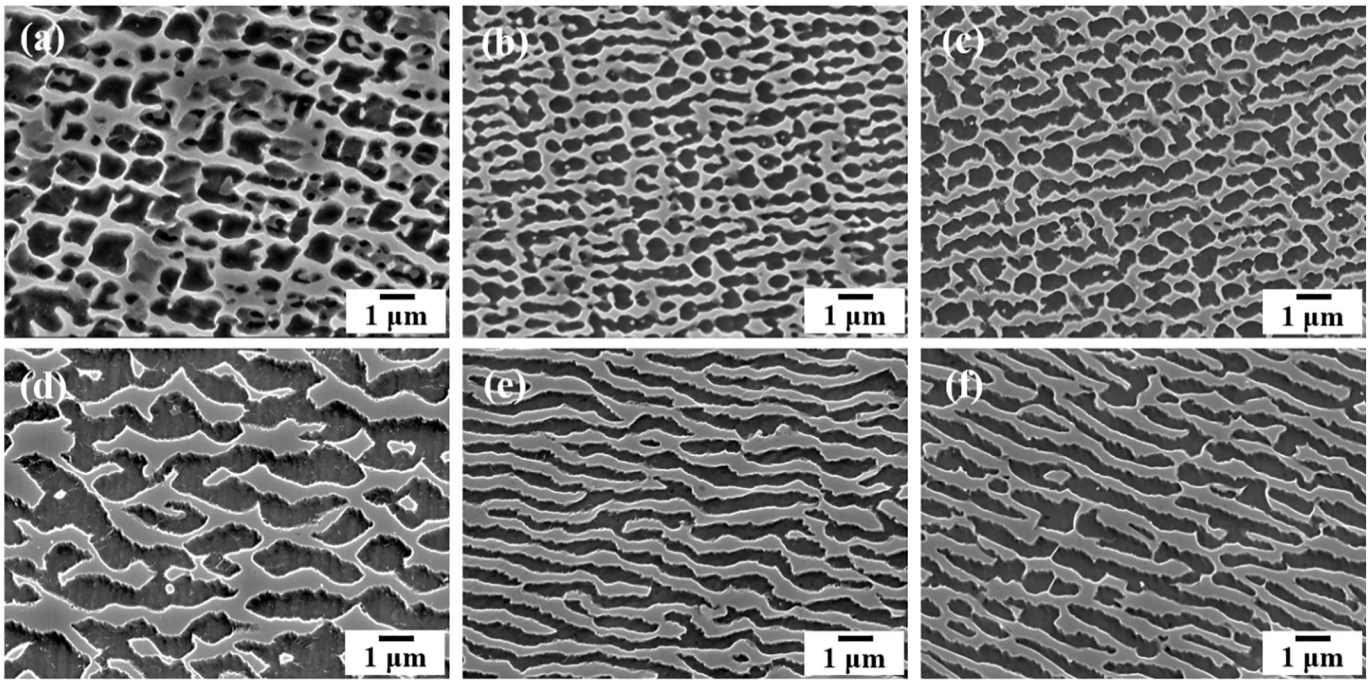

Fig. 11. Morphologies of γ′ particles after creep test at 871 °C/320 MPa ((a), (b), (c)) and 982 °C/165 MPa ((d), (e), (f)), with different heat treatments, (a) HT2, (b) HT3, (c) HT4, (d) HT1, (e) HT3, and (f) HT4.

the effect of inhibiting dislocation movement in octocube or cube form γ′ was not significantly different at this temperature. When the creep behaviors of HT3 and HT4 specimens at intermediate and high temperatures were compared, the differences in creep lives were not large, unlike at low-temperature and high-stress conditions. A large number of finely precipitated primary γ′ in the dendrite core was more effective in suppressing dislocation movement, but the role of eutectic γ/γ′ in suppressing stress concentration and relieving damage became less important at high temperatures.

4. Conclusions

The effect of the precipitation behavior of γ′ particles and dissolution of eutectic γ/γ′ phase on the creep deformation due to the heat treatment of a conventionally cast superalloy CM 247 LC have been studied. The conclusions are summarized as follow:

(1) The precipitation behavior of secondary γ′ particles depends on heat treatment path. A large amount of secondary γ′ formed in the two-step-aging specimen not subjected to the solution treatment (HT2), whereas almost no secondary γ′ formed in the aged specimen after the solution treatment (HT3 and HT4). The width of γ channel in the HT2 specimen was wider than HT3 and HT4 specimens because volume fraction of γ′ was smaller, and the size of γ′ was larger. Therefore, secondary γ′ particles grew and remained in the wider channel rather than being absorbed into primary γ′ during secondary aging.
(2) The eutectic γ/γ′ was found to act as a barrier to prevent dislocation movement when dislocation cut through the γ′ particles. The eutectic phase suppressed progress of the slip band and relieved the concentration of deformation into a specific region.
(3) The creep properties of the two step aging specimens (HT2) were the best at low temperature and high stress conditions (760 °C/620 MPa), because the deformation was uniform and the damage was mitigated due to the eutectic γ/γ′ phases and fine secondary γ′ in the γ channel.
(4) At temperatures above 871 °C, creep properties were much more affected by the rafting of primary γ′ particles than by the precipitation of secondary γ′, and creep lifetimes of solution treated specimens with good rafting were longer than those of aged specimens with poor rafting.

Declaration of competing interest

The authors declare that they have no known competing financial interests or personal relationships that could have appeared to influence the work reported in this paper.

Acknowledgements

This work was supported by “Power Generation & Electricity Delivery (No. 20181110100310)” of the Korea Institute of Energy Technology Evaluation and Planning (KETEP) and granted financial resources from the Ministry of Trade, Industry and Energy, Korea and by the Fundamental Research Program of the Korea Institute of Materials Science (KIMS, No. PNK6120).

References

[1] K. Harris, G.L. Erickson, R.E. Schwer, Mar M 247 derivations – CM 247 LC DS alloy and CMSX4 single crystal alloys: Properties and performance, in: M. Gell (Ed.), Superalloys 1984: Proceedings of Fifth International Symposium on Superalloys, Metallurgical Society of AIME, Warrendale (Pennsylvania, 1984, pp. 221–230.
[2] T. Murakumo, T. Kobayashi, Y. Koizumi, H. Harada, Creep behaviour of Ni-base single-crystal superalloys with various γ′ volume fraction, Acta Mater. 52 (12) (2004) 3737–3744, https://doi.org/10.1016/j.actamat.2004.04.028.
[3] T. Wang, X. Wang, Z. Zhao, Z. Zhang, Dissolution behaviour of the γ′ precipitates in two kinds of Ni-based superalloys, Mater. High Temp. 33 (1) (2016) 51–57, https://doi.org/10.1179/1878641315Y.0000000006.
[4] G.L. Erickson, K. Harris, R.E. Schwer, Directionally solidified DS CM 247 LC - optimized mechanical properties resulting from extensive γ′ solutioning, ASME 1985 International Gas Turbine Conference and Exhibit 85-GT-107, The American Society of Mechanical Engineers, New York, 1985, pp. 1–10, , https://doi.org/10.1115/85-GT-1075.
[5] H.-E. Huang, C.-H. Koo, Characteristics and mechanical properties of polycrystalline CM247LC superalloy castings, Mater. Trans. Japan 45 (2) (2004) 562–568, https://doi.org/10.2320/matertrans.45.562.
[6] S.A. Sajjadi, S. Nategh, A high temperature deformation mechanism map for the high performance Ni-base superalloy GTD-111, Mater. Sci. Eng. A 307 (1–2) (2001)

158–164, https://doi.org/10.1016/S0921-5093(00)01822-0.
[7] L. Shui, T. Jin, S. Tian, Z. Hu, Influence of precipitate morphology on tensile creep of a single crystal nickel-base superalloy, Mater. Sci. Eng. A 454–455 (2007) 461–466, https://doi.org/10.1016/j.msea.2006.11.136.
[8] R. Baldan, R.L.P. da Rocha, R.B. Tomasiello, C.A. Nunes, A.M.S. Costa, M.J.R. Barboza, G.C. Coelho, R. Rosenthal, Solutioning and aging of MAR-M247 nickel-based superalloy, J. Mater. Eng. Perform. 22 (9) (2013) 2574–2579, https://doi.org/10.1007/s11665-013-0565-4.
[9] M. Rahimian, S. Milenkovic, I. Sabirov, Microstructure and hardness evolution in MAR-M247 Ni-based superalloy processed by controlled cooling and double heat treatment, J. Alloys Compd. 550 (2013) 339–344, https://doi.org/10.1016/j.jallcom.2012.10.129.
[10] R.K. Rai, J.K. Sahu, A. Parmanick, N. Paulose, D.C. Fernando, S.K. Das, Creep deformation micro-mechanisms of CM 247DS LC Ni-base superalloy under relevant service condition, Mater. Charact. 150 (2019) 155–165, https://doi.org/10.1016/j.matchar.2019.02.021.
[11] J.J. Jackson, M.J. Donachie, M. Gell, R.J. Henricks, The effect of volume percent of fine γ′ on creep in DS Mar-M 200 + Hf, Metall. Trans. A. 8 (10) (1977) 1615–1620, https://doi.org/10.1007/BF02644867.
[12] B. Décamps, S. Raujol, A. Coujou, F. Pettinari-Sturmel, N. Clément, D. Locq, P. Caron, On the shearing mechanism of γ′ precipitates by a single a/6<112> Shockley partial in Ni-based superalloys, Philos. Mag. A 84 (1) (2004) 91–107, https://doi.org/10.1080/14786430310001621472.
[13] K.L. Gasko, G.M. Janowski, B.J. Pletka, The influence of γ-γ′ eutectic on the mechanical properties of conventionally cast Mar-M247, Mater. Sci. Eng. A 104 (1988) 1–8, https://doi.org/10.1016/0025-5416(88)90400-4.
[14] J.E. Doherty, B.H. Kear, A.F. Giamei, On the origin of the ductility enhancement in Hf-doped Mar-M200, J. Met. 23 (11) (1971) 59–62, https://doi.org/10.1007/BF03355744.
[15] D.N. Duhl, C.P. Sullivan, Some effects of hafnium additions on the mechanical properties of a columnar-grained nickel-base superalloy, J. Met. 23 (7) (1971) 38–40, https://doi.org/10.1007/BF03355714.
[16] U. Tetzlaff, H. Mughrabi, Enhancement of the high-temperature tensile creep strength of monocrystalline nickel-base superalloys by pre-rafting in compression, in: T.M. Pollock, R.D. Kissinger, R.R. Bowman, K.A. Green, M. McLean, S. Olson, J.J. Schirra (Eds.), Superalloys 2000, the Minerals, Metals &Materials Society, Warrendale, Pennsylvinia, 2000, pp. 273–282.
[17] C.M.F. Rae, R.C. Reed, Primary creep in single crystal superalloys: origin, mechanisms and effects, Acta Mater. 55 (2007) 1067–1081, https://doi.org/10.1016/j.actamat.2006.09.026.
[18] L. Cui, J. Yu, J. Liu, T. Jin, X. Sun, The creep deformation mechanisms of a newly designed nickel-base superalloy, Mater. Sci. Eng. A 710 (2018) 309–317, https://doi.org/10.1016/j.msea.2017.11.002.
[19] T. Murakumo, Y. Koizumi, K. Kobayashi, H. Harada, Creep strength of Ni-base single crystal superalloys on the γ/γ′ tie-line, in: K.A. Green, T.M. Pollock, H. Harada, T.E. Howson, R.C. Reed, J.J. Schirra, S. Walston (Eds.), Superalloys 2004, the Minerals, Metals &Materials Society, Warrendale, Pennsylvinia, 2004, pp. 155–162.
[20] P. Caron, T. Khan, Improvement of creep strength in a nickel-base single-crystal superalloy by heat treatment, Mater. Sci. Eng. 61 (2) (1983) 173–184, https://doi.org/10.1016/0025-5416(83)90199-4.
[21] X.G. Wang, J.L. Liu, T. Jin, X.F. Sun, Y.Z. Zhou, Z.Q. Hu, J.H. Do, B.G. Choi, I.S. Kim, C.Y. Jo, Creep deformation related to dislocations cutting the phase of a Ni-base single crystal superalloy, Mater. Sci. Eng. A 626 (2015) 406–414, https://doi.org/10.1016/j.msea.2014.12.060.